

Deep Learning Based Multi-Step Channel Prediction for Adaptive Underwater Acoustic OFDM Systems

Tian Tian ^{*}, Ying Zhang [†], Agastya Raj ^{*}, Fei-Yun Wu [§], Marco Ruffini ^{*}

^{*} IRIS Research Group, ADAPT Center, School of Computer Science and Statistics, Trinity College Dublin, Ireland

[†] College of Oceanography, Hohai University, Nanjing, Jiangsu, China

[§] Navigation College, Jimei University, Xiamen, Fujian, China

Abstract—We develop an adaptive OFDM framework for underwater acoustic communications based on PatchCSI-T, a Transformer-based multistep channel prediction model with feature-independent modeling and parameter sharing. Combined with a greedy adaptive modulation and power allocation scheme, the proposed approach enables accurate, low-latency CSI forecasting and improves end-to-end BER and spectral efficiency on real-world UWA channel datasets.

I. INTRODUCTION

Acoustic propagation in the ocean is governed by frequency-dependent attenuation, severe time-varying multipath fading, motion-induced Doppler shifting and long propagation delays that are more pronounced due to the low sound speed [1]. These characteristics make timely Channel State Information (CSI) acquisition difficult as round-trip propagation delays over kilometer-scale links can reach seconds, rendering feedback-based link adaptation impractical when the channel coherence time is of similar order.

Channel prediction mitigates feedback latency by enabling proactive link adaptation without waiting for round-trip CSI feedback. Accurate multi-step-ahead CSI prediction allows adaptive communication systems to operate on predicted rather than outdated channel conditions, thereby improving spectral efficiency and reducing Bit Error Rate (BER) [2]. Conventional adaptive filtering methods, such as Recursive Least Squares (RLS), have been widely used for Underwater Acoustic (UWA) channel estimation and prediction [3]. However, these methods often struggle to capture the nonlinear and rapidly time-varying characteristics of UWA channels.

Recently, Deep Learning (DL)-based methods have shown potential for UWA channel prediction. Existing studies include hybrid CNN-RNN architectures for CSI prediction in adaptive downlink OFDMA systems [4], attention-based recurrent models for capturing long-range temporal dependencies in time-varying channels [5], bidirectional GRU-based models for UWA MIMO systems [6], and Multi-Task Learning (MTL) frameworks for high-dimensional Channel Impulse Response (CIR) prediction [7]. However, current DL-based channel prediction methods still face important limitations. RNN-based architectures that rely on autoregressive multi-step prediction suffer from error accumulation, as prediction errors propagate and amplify over long horizons. In addition, architectures that employ cross-dimension feature mixing to capture inter-subcarrier or inter-tap correlations are prone to overfitting when training data are limited, which is a common constraint

in UWA applications due to the high cost of at-sea measurements.

Motivated by the limitations of existing methods, this paper proposes an adaptive OFDM framework with two key components: (1) PatchCSI-T, a Transformer-based multi-step channel prediction model inspired by time-series forecasting model PatchTST [8], which leverages patching, feature-independent modeling, and parameter sharing to reduce attention complexity and mitigate overfitting; and (2) a greedy adaptive modulation and power allocation scheme that jointly selects the modulation order and transmit power to satisfy a target BER while maximizing spectral efficiency. Experiments on field-measured UWA channel datasets show that PatchCSI-T outperforms state-of-the-art baselines in both prediction accuracy and inference efficiency. When integrated into the adaptive OFDM system, the proposed framework further improves end-to-end BER and spectral efficiency.

II. SYSTEM MODEL AND PROPOSED FRAMEWORK

The overall system framework and the structure of the PatchCSI-T channel prediction model are shown in Fig. 1. The transmitter adaptively maps input bits onto \mathcal{M} -ary symbols according to the predicted CSI, applies per-subcarrier power loading, and converts the signal to the time domain via IFFT. At the receiver, after frame synchronization and FFT processing, channel estimation and equalization are performed, followed by symbol demapping to recover the transmitted bits.

A. Problem Formulation

Consider an OFDM system with N_f subcarriers. Let G_i denote the complex channel gain on subcarrier i and C_i the power allocated to that subcarrier. Each subcarrier employs an \mathcal{M}_i -ary modulation, with modulation order \mathcal{M}_i corresponding to $b_i = \log_2 \mathcal{M}_i$ bits per symbol. The adaptive modulation and power allocation problem seeks to maximize throughput subject to a total power budget C^{budget} , a target BER P_b^{target} , and a per-subcarrier modulation constraint:

$$\max \sum_{i=1}^{N_f} b_i \text{ s.t. } \sum_{i=1}^{N_f} C_i \leq C^{\text{budget}}, \frac{1}{N_f} \sum_{i=1}^{N_f} P_{b,i} \leq P_b^{\text{target}}, b_i \leq b^{\text{max}}. \quad (1)$$

For a given modulation order \mathcal{M}_i and per-subcarrier Signal-to-Noise Ratio (SNR) $\gamma_i = C_i |G_i|^2 / N_0$, the BER of \mathcal{M}_i -ary modulation can be approximated as [3]:

$$P_{b,i}(\gamma_i, \mathcal{M}_i) \approx 0.2 \exp(-q(\mathcal{M}_i)\gamma_i) \quad (2)$$

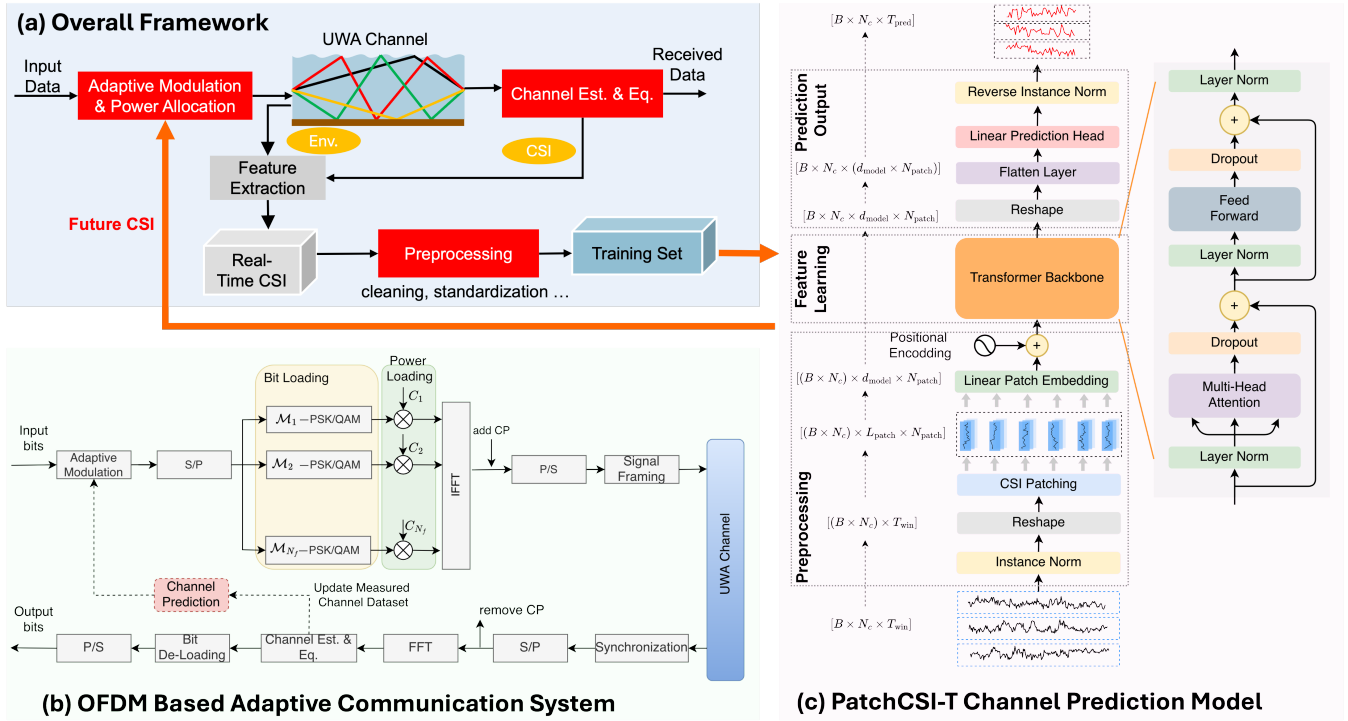


Fig. 1: System framework and channel prediction model.

where $q(\mathcal{M}_i)$ is a modulation-dependent constant with values $q(\mathcal{M}_i) = 1.1, 0.55, 0.25, 0.12$ for $\mathcal{M}_i = 2, 4, 8, 16$, respectively. Since the system operates based on predicted rather than perfect CSI, the prediction error is modeled as $e_i = \hat{G}_i - G_i$, where \hat{G}_i denotes the predicted channel gain and $e_i \sim \mathcal{CN}(0, \sigma_e^2)$. Under the Gaussian error model, the conditional expected BER on subcarrier i is

$$\mathbb{E}[P_{b,i}|\hat{G}_i] = 0.2 \frac{\exp\left(-\frac{|\hat{G}_i|^2}{\sigma_e^2} \left(1 - \frac{1}{1+q(\mathcal{M}_i)\frac{C_i}{N_0}\sigma_e^2}\right)\right)}{1+q(\mathcal{M}_i)\frac{C_i}{N_0}\sigma_e^2} \quad (3)$$

Imposing the constraint $\mathbb{E}[P_{b,i}|\hat{G}_i] \leq P_b^{\text{target}}$ and solving for C_i , a closed-form minimum power threshold can be obtained in terms of the Lambert-W function $W_0(\cdot)$ [3]:

$$C_{\text{thre},i}(\mathcal{M}_i, \hat{G}_i, P_b^{\text{target}}) = \frac{N_0}{q(\mathcal{M}_i)\sigma_e^2} \left[\frac{|\hat{G}_i|^2}{\sigma_e^2} W_0\left(\frac{P_b^{\text{target}}}{0.2} \exp\left(\frac{|\hat{G}_i|^2}{\sigma_e^2}\right) \frac{|\hat{G}_i|^2}{\sigma_e^2}\right)^{-1} - 1 \right] \quad (4)$$

This threshold represents the minimum transmit power required on subcarrier i to satisfy target BER for a chosen modulation order \mathcal{M}_i , accounting for CSI prediction uncertainty.

B. Greedy Bit / Power Allocation

Directly solving (1) is computationally expensive. We therefore employ a low-complexity greedy algorithm that iteratively adjusts per-subcarrier modulation orders using the power

threshold (4). At each iteration n , the most efficient bit upgrade is identified by:

$$i^* = \arg \min_{1 \leq i \leq N_f} (\Delta C_i^{(n)}), \quad (5)$$

$$\Delta C_i^{(n)} = C_{\text{thre},i}(2^d \mathcal{M}_i^{(n)}, \hat{G}_i^{(n)}, P_b^{\text{target}}) - C_i^{(n)}$$

where the subcarrier that requires the smallest incremental power is selected. This greedy process repeats, using the predicted CSI to recompute required power for each subcarrier, until the power budget is exhausted or no further upgrade satisfies P_b^{target} . If the channel conditions deteriorate, the algorithm downgrades the subcarrier with the largest marginal cost (i.e., set $d = -1$ in (5)).

C. Channel Prediction Model

The multi-step channel prediction problem aims to forecast future CSI $\{\mathbf{h}^{[t+1]}, \dots, \mathbf{h}^{[t+T_{\text{pred}}]}\}$ from a historical observation window $\{\mathbf{h}^{[t-T_{\text{win}}+1]}, \dots, \mathbf{h}^{[t]}\}$, where each $\mathbf{h}^{[t]} \in \mathbb{R}^{N_c}$ is a CSI vector with N_c features (e.g., multipath taps or subcarrier gains). PatchCSI-T adopts a joint multi-step prediction strategy, generating the entire T_{pred} -step future sequence in a single forward pass to avoid the error accumulation inherent in recursive approaches.

Let $\mathbf{X} \in \mathbb{R}^{N_c \times T_{\text{win}}}$ denote the input CSI matrix formed by stacking the historical CSI vectors over the observation window, where the k -th row $\mathbf{x}^{(k)} = \mathbf{X}(k, :) \in \mathbb{R}^{T_{\text{win}}}$ represents the temporal sequence of the k -th CSI feature. Instead of processing each time sample independently, PatchCSI-T partitions each feature sequence $\mathbf{x}^{(k)}$ into overlapping patches

of length L_{patch} with stride s_{patch} , yielding $N_{\text{patch}} = \lfloor (T_{\text{win}} - L_{\text{patch}}) / s_{\text{patch}} \rfloor + 2$ tokens after end-padding. This reduces the effective sequence length from T_{win} to N_{patch} , lowering the self-attention complexity from $O(T_{\text{win}}^2)$ to $O(N_{\text{patch}}^2)$, while enabling the model to capture temporal dependencies at the segment level rather than between isolated time samples. Each patch is then mapped to a d_{model} -dimensional space via a linear embedding and combined with sinusoidal positional encoding.

At the core of PatchCSI-T is the Transformer encoder layer which globally models the relationships among all patch tokens. Existing channel prediction methods often adopt feature-mixing modeling to capture inter-feature correlations (e.g., across multipath taps or subcarriers). However, recent studies in time-series forecasting suggest that feature-independent modeling is often more robust [9], especially when inter-feature correlations are weak or non-stationary. Moreover, feature mixing increases model complexity and data requirements, which can aggravate overfitting when training data are limited. PatchCSI-T therefore adopts feature-independent modeling. Specifically, as shown in Fig. 1(c), the feature dimension N_c is merged into the batch dimension B , yielding $\mathbf{X} \in \mathbb{R}^{(BN_c) \times L_{\text{patch}} \times N_{\text{patch}}}$ after patching. This allows all features to be processed in parallel within a single forward pass. Although features are processed independently, they share the same model parameters and are optimized jointly. Finally, the backbone output is flattened and passed to a linear prediction head that directly generates the full T_{pred} -step future sequence:

$$\mathbf{X}_{\text{out}}^{(k)} = \mathbf{W}_P \text{Flatten}(\mathbf{R}^{(k)}) + \mathbf{b}_P \quad (6)$$

where $\mathbf{W}_P \in \mathbb{R}^{T_{\text{pred}} \times (d_{\text{model}} \times N_{\text{patch}})}$, $\mathbf{b}_P \in \mathbb{R}^{T_{\text{pred}}}$ are learnable parameters.

III. NUMERICAL RESULTS

A. Dataset and Experimental Setup

We evaluate the performance using the open-access China-Wanlu Reservoir dataset [10], which includes 2,137 CIR measurements with maximum delay spread of $\tau_{\text{max}} = 20$ ms and $N_\tau = 120$ multipath taps. To assess frequency-domain prediction performance, we apply Fourier transform to the CIR data, corresponding to a bandwidth of $BW = N_\tau / \tau_{\text{max}} = 6$ kHz and $N_f = 256$ subcarrier bins in Channel Frequency Response (CFR). Fig. 2 illustrates both the time-varying characteristics of the CIR and CFR. The dataset is partitioned into 70% training, 10% validation, and 20% test sets in chronological order.

For the PatchCSI-T model, the patch length is set to $L_{\text{patch}} = 16$, the stride to $s_{\text{patch}} = 8$, corresponding to 50% overlap, and the hidden dimension to $d_{\text{model}} = 64$. The model is trained using the Root Mean-Square Error (RMSE) loss with a historical window of $T_{\text{win}} = 64$. Prediction accuracy is measured by Normalized Mean-Square Error (NMSE):

$$\text{NMSE} = \frac{1}{N_s} \sum_{n=1}^{N_s} \frac{\|\hat{\mathbf{y}}^{[n]} - \mathbf{y}^{[n]}\|_2^2}{\|\mathbf{y}^{[n]}\|_2^2}, \quad (7)$$

where $\mathbf{y}^{[n]}$, $\hat{\mathbf{y}}^{[n]} \in \mathbb{R}^{N_f}$ denote the ground-truth and predicted CFR vectors corresponding to the n -th sample in the test set, and N_s denotes the total number of test samples.

We compare PatchCSI-T against RLS, BiGRU [6], CNN1d-LSTM [4], and MTL-LSTM [7]. For the DL baselines, d_{model} is selected by hyperparameter search over $\{64, 128, 256\}$, resulting in $d_{\text{model}} = 64$ for MTL-LSTM and $d_{\text{model}} = 256$ for BiGRU and CNN1d-LSTM. All DL models are trained under the same protocol using the AdamW optimizer. Experiments are conducted on a workstation equipped with an NVIDIA GeForce RTX 4090 GPU, a 13th Gen Intel Core i9-13900K CPU, and 64 GB RAM.

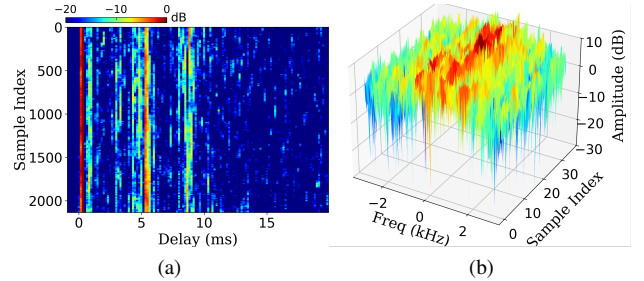


Fig. 2: Time-varying channel dataset: (a) CIRs, (b) CFRs.

B. Prediction Performance Analysis

Fig. 3 summarizes CFR predictions over horizons $T_{\text{pred}} \in \{2, 4, 8, 16, 32, 64, 128\}$, including NMSE, per-epoch training time (T_{epoch}) and inference time (T_{pred}). PatchCSI-T consistently achieves higher accuracy and faster inference. At $T_{\text{pred}} = 32$, it attains -14.76 dB NMSE, a 1.4-4.9 dB NMSE gain over the baselines, with 14.7 ms inference ($\sim 6\times$ faster than CNN1d-LSTM/BiGRU and $> 50\times$ faster than MTL-LSTM). Notably, CNN1d-LSTM and BiGRU exhibit NMSE saturation near -10 dB for large prediction horizon T_{pred} , as these models were originally developed for single-step prediction tasks on larger datasets (e.g., CsiPreNet employs a similar CNN1d-LSTM structure trained on 10,584 samples for 34 subcarrier clusters [4]).

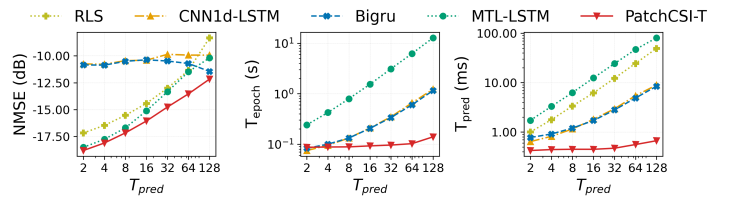


Fig. 3: Comparison of prediction performance.

To understand how PatchCSI-T captures temporal dependencies, Fig. 4 shows the multi-head attention weight matrices, averaged over all attention heads, together with the corresponding multi-step prediction curves for selected CFR subcarrier features. In this example, the model uses $T_{\text{win}} = 256$ and $T_{\text{pred}} = 4$. The feature-independent strategy enables the model to learn distinct attention patterns for channel components

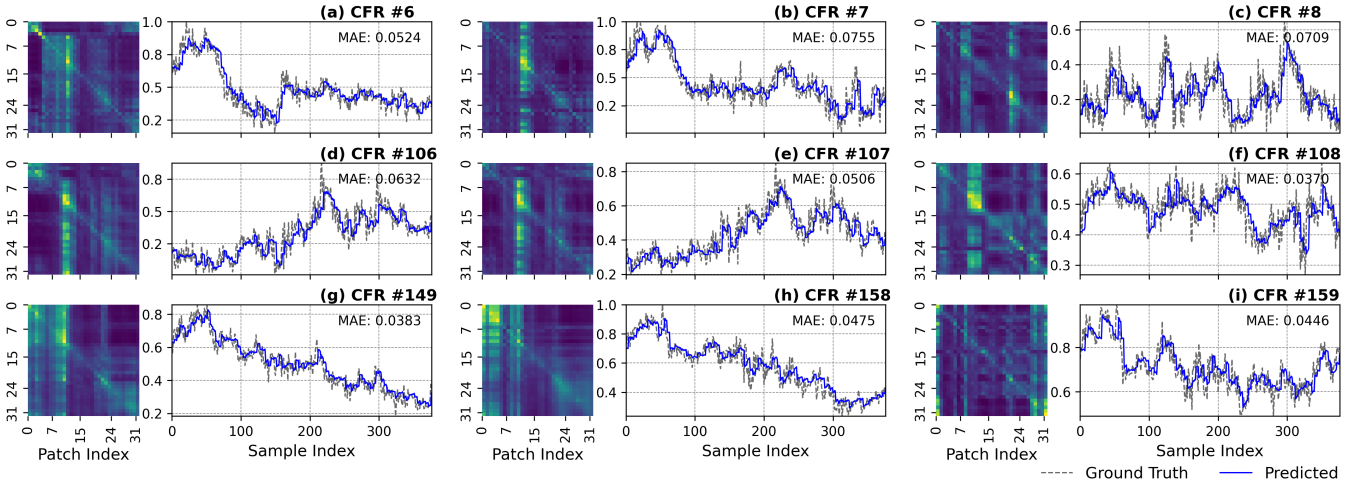


Fig. 4: Multi-head attention weight matrices and prediction curves for selected subcarrier components.

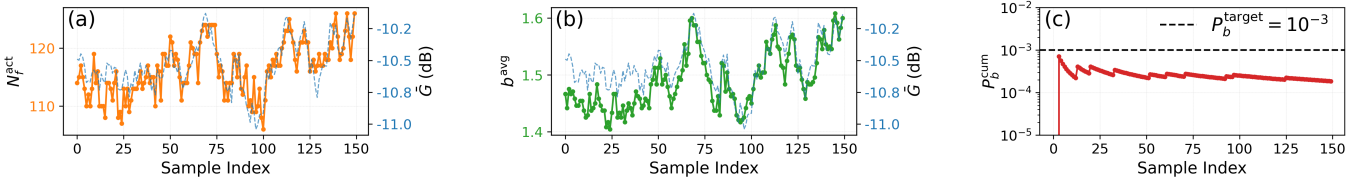


Fig. 5: Performance of the adaptive OFDM scheme under ground-truth CFR at SNR=5 dB: (a) number of active subcarriers N_f^{act} and average channel gain \bar{G} ; (b) average number of bits per data subcarrier b^{avg} ; and (c) cumulative BER P_e^{cum} .

with different temporal characteristics. Features with similar temporal dynamics, such as adjacent subcarriers experiencing correlated fading, exhibit similar attention structures. This indicates that the shared Transformer backbone can capture feature-specific temporal dependencies without explicit cross-feature modeling.

C. Performance in Adaptive OFDM System

The OFDM system is configured with $N_f = 256$ subcarriers over a bandwidth of $B_W = 6$ kHz, corresponding to a subcarrier spacing of $\Delta f = 23.4$ Hz. Among them, 240 subcarriers are allocated for data transmission and 16 are null subcarriers reserved for guard bands and noise monitoring. The OFDM symbol duration is $T_{\text{OFDM}} = 42.7$ ms, with a cyclic prefix of $T_{\text{CP}} = 20$ ms. Each data subcarrier is assigned one of five states: deactivated, BPSK, QPSK, 8PSK, or 16QAM. The target bit error rate is set to $P_b^{\text{target}} = 10^{-3}$. Subcarriers that cannot support even BPSK at the target BER are deactivated, and their power is reallocated to the remaining active subcarriers.

We first validate the greedy modulation and power allocation algorithm using ground-truth CFR. Fig. 5 shows the temporal evolution of the allocation results together with the average channel gain \bar{G} . As shown in Fig. 5 (a) and (b), both the number of active subcarriers N_f^{act} and the average number of bits per data subcarrier b^{avg} closely track the variation of \bar{G} : when the average channel gain increases, more subcarriers are activated and higher-order modulation levels are selected. During channel fades, the number of active subcarriers and the

modulation order are reduced to maintain the target BER. Fig. 5 (c) shows that the cumulative BER remains well below 10^{-3} , confirming that the adaptive algorithm can maintain reliable transmission under time-varying channel conditions.

We next evaluate the adaptive OFDM system under predicted CFR. The channel prediction horizon is $T_{\text{pred}} = 32$. Fig. 6 shows the BER distribution across three SNR levels using both ground-truth and predicted CFR from each model. Fig. 7 plots the effective spectral efficiency (SE) defined as

$$SE = \frac{\sum_{n=1}^{N_s} \sum_{i=1}^{N_f} I(P_b^{(n)} < P_b^{\text{target}}) \log_2 \mathcal{M}_i^{(n)}}{N_s \times B_W \times (T_{\text{OFDM}} + T_{\text{CP}})}. \quad (8)$$

Across all SNR levels, PatchCSI-T achieves performance closest to ground truth CSI. For instance, at SNR=15dB, PatchCSI-T maintains 89.7% of transmitted symbols with $P_b^{\text{target}} \leq 10^{-3}$ and 5.14 bps/Hz spectral efficiency, outperforming RLS (72.9%, 4.15 bps/Hz) and MTL-LSTM (75.8%, 4.34 bps/Hz).

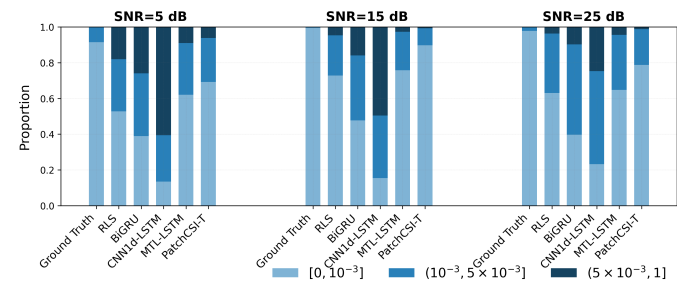


Fig. 6: BER distribution under real and predicted CFRs.

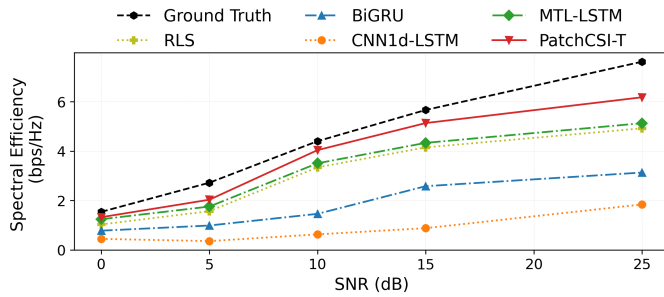


Fig. 7: Spectral efficiency for the adaptive OFDM system.

IV. CONCLUSIONS

This paper presents PatchCSI-T, a joint multi-step CSI prediction model for adaptive OFDM in time-varying UWA channels. Results on the open-access China-Wanlu Reservoir dataset show that PatchCSI-T improves prediction accuracy by 1.4–4.9 dB in NMSE at horizon $T_{\text{pred}} = 32$ over the baselines, while reducing inference time by more than $50\times$ compared with MTL-LSTM. Integrated with a greedy modulation and power allocation scheme, the proposed framework achieves 5.14 bps/Hz spectral efficiency at SNR = 15 dB, with 89.7% of transmitted symbols satisfying the target BER. Future work will extend validation to at-sea data with stronger Doppler and longer delays, and to real-time closed-loop experiments.

V. ACKNOWLEDGMENT

This work was supported in part by the National Natural Science Foundation of China under Grants 42306207 and 62171369, in part by the National Key Research and Development Program of China under Grant 2024YFF0510000, in part by the Natural Science Foundation of Fujian Province under Grant 2025J01860, and in part by the Research Ireland Sea-Scan project under grant 24/FIP/DO/13340P and 13/RC/2106_P2 (ADAPT centre) and 18/RI/5721 (OpenIreland Research Infrastructure).

REFERENCES

- [1] M. Stojanovic and J. Preisig, "Underwater acoustic communication channels: Propagation models and statistical characterization," *IEEE Commun. Mag.*, vol. 47, no. 1, pp. 84–89, Jan. 2009.
- [2] L. Huang, Q. Zhang, L. Zhang, J. Shi, and L. Zhang, "Efficiency Enhancement for Underwater Adaptive Modulation and Coding Systems: Via Sparse Principal Component Analysis," *IEEE Commun. Lett.*, vol. 24, no. 8, pp. 1808–1811, Aug. 2020.
- [3] A. Radosevic, R. Ahmed, T. M. Duman, J. G. Proakis, and M. Stojanovic, "Adaptive OFDM Modulation for Underwater Acoustic Communications: Design Considerations and Experimental Results," *IEEE J. Ocean. Eng.*, vol. 39, no. 2, pp. 357–370, Apr. 2014.
- [4] L. Liu, L. Cai, L. Ma, and G. Qiao, "Channel State Information Prediction for Adaptive Underwater Acoustic Downlink OFDMA System: Deep Neural Networks Based Approach," *IEEE Trans. Veh. Technol.*, vol. 70, no. 9, pp. 9063–9076, September 2021.
- [5] Z. Zhu, F. Tong, Y. Zhou, Z. Zhang, and F. Zhang, "Deep Learning Prediction of Time-Varying Underwater Acoustic Channel Based on LSTM with Attention Mechanism," *J. Marine. Sci. Appl.*, vol. 22, no. 3, pp. 650–658, Sep. 2023.
- [6] X. Hu, Y. Huo, X. Dong, F.-Y. Wu, and A. Huang, "Channel Prediction Using Adaptive Bidirectional GRU for Underwater MIMO Communications," *IEEE Internet Things J.*, pp. 1–1, 2023.

- [7] T. Tian, A. Raj, B. M. Xavier, Y. Zhang, F.-Y. Wu, and K. Yang, "A multi-task learning framework for underwater acoustic channel prediction: Performance analysis on real-world data," *IEEE Trans. Wireless Commun.*, vol. 23, no. 11, pp. 15 930–15 944, 2024.
- [8] Y. Nie, N. H. Nguyen, P. Sinthong, and J. Kalagnanam, "A Time Series is Worth 64 Words: Long-term Forecasting with Transformers," Mar. 2023.
- [9] L. Han, H.-J. Ye, and D.-C. Zhan, "The Capacity and Robustness Trade-Off: Revisiting the Channel Independent Strategy for Multivariate Time Series Forecasting," *IEEE Trans. Knowl. Data Eng.*, vol. 36, no. 11, pp. 7129–7142, Nov. 2024.
- [10] H. Zhao, F. Ji, Q. Li, Q. Guan, S. Wang, and M. Wen, "Federated Meta-Learning Enhanced Acoustic Radio Cooperative Framework for Ocean of Things," *IEEE J. Sel. Top. Signal Process.*, vol. 16, no. 3, pp. 474–486, Apr. 2022.